Journal of Nuclear Materials 459 (2015) 30–36

Contents lists available at ScienceDirect

Journal of Nuclear Materials

journal homepage: www.elsevier.com/locate/jnucmat

# DFT-based Metadynamics simulation of proton diffusion in tetragonal zirconia at 1500 K

Jeremy Rabone *, Paul Van Uffelen

*European Commission, Joint Research Centre, Institute for Transuranium Elements, D-76125 Karlsruhe, Germany*

ARTICLE INFO

*Article history:*
Received 11 March 2014
Accepted 3 January 2015
Available online 9 January 2015

ABSTRACT

The diffusion rate of hydrogen in zirconium oxides comes into play in both the steam oxidation and the hydriding of zirconium alloys. In view of the low measured uptake and diffusion of neutral hydrogen species in zirconium oxides, it has been suggested that the measured rates of hydrogen uptake in zircaloys exposed to high-temperature steam can be explained by the diffusion of protons through the surface oxide layers. This paper investigates the diffusion of protons in tetragonal zirconia at 1500 K using density functional theory-based molecular dynamics and Metadynamics simulations. An average value of $4 \times 10^{-9}/m^2\ s^{-1}$ is calculated for the diffusion rate, which, considering the contrived basis of the simulations, compares qualitatively with the value of $3.2 \times 10^{-10}/m^2\ s^{-1}$ obtained by fit to experimentally-determined diffusivities of hydrogen in yttrium-stabilized zirconia. The simulations described show that the "proton" is present as the hydrogen atom in a hydroxide ion, and the analysis of the electronic structure reveals that the diffusion of the proton is mediated by two-electron-three-centre bonds that form between hydroxide and adjacent oxide ions.



## 1. Introduction

The vast majority of commercial nuclear fuel rods make use of zircaloy as cladding materials for containing the oxide fuel pellets in which the radioactive fission products are produced. In the event of a loss of coolant accident, the temperature surrounding the fuel rods will increase, thereby accelerating the interaction rate of the zircaloy with the remaining coolant or steam. The exothermic interaction produces hydrogen, part of which can be absorbed in the cladding. The uptake of hydrogen into the zirconium alloys is also of interest during normal operating conditions, as the resulting embrittlement of the cladding through the formation of hydrides is a consideration for operational safety.

The safety analysis requires an accurate understanding of the basic mechanisms involved in addition to the quantification of the dominant process parameters. Despite the large amount of experimental investigations and model developments carried out until now, there remain some open questions about the basic mechanism that controls the high temperature oxidation of the zircaloy cladding by interaction with steam. It has been suggested [1] that the observed transport rates of hydrogen through the surface zirconia layer and high temperature [2–6] are evidence that the diffusing species are protons (in the chemical rather than the physical sense, the term proton and hydrogen atom are used interchangeably in this manuscript). Conversely, measurements of gaseous hydrogen uptake and diffusion in zirconia point to sorption of hydrogen as neutral species with very low solubilities and mobility [7]. The uptake of steam in yttrium stabilized zirconia has been explained as a reaction between charged vacancies and water molecules, so filling the vacancies with oxide ions and leaving proton interstitials [8].

Density functional theory (DFT) calculations have recently been applied to the diffusion of hydrogen in zirconia [9]. These calculations, however, considered the diffusion of neutral hydrogen in a fixed zirconia structure which confines their applicability to lower temperature regimes where the effects of lattice vibrations on the diffusion motion can be treated in the harmonic approximation. To build a more complete picture of high-temperature hydrogen diffusion in zirconia, we have applied DFT-based molecular dynamics (MD) and accelerated dynamics (Metadynamics) to the diffusion of protons in tetragonal zirconia. The combination of DFT with MD allows an accurate treatment of the electronic interactions and forces while concurrently allowing for the relatively large atomic motions at high temperatures.

The structure of the paper is as follows. After providing details about the computational method (Section 1.1), the validation of the model parameters is outlined based on a comparison with a second DFT code as well as with experimental data (Section 1.2). The model is then applied to simulate the migration of protons

* Corresponding author. Tel.: +49 7247 951297.
*E-mail address:* jeremy.rabone@ec.europa.eu (J. Rabone).

http://dx.doi.org/10.1016/j.jnucmat.2015.01.002
0022-3115/

with an emphasis on understanding the underlying mechanisms (Section 2).

### 1.1. Computational methods

The calculations were carried out using the QUICKSTEP [10,11] module of CP2K (development version 2.2.214) [12] with a mixed Gaussian and plane waves basis [13]. Periodic boundary conditions were applied in all three dimensions. The spin-unpolarized PBE functional was used [14] with Goedecker–Teter–Hutter (GTH) pseudopotentials [15–17] incorporating scalar-relativistic core corrections. The orbital transformation method [18] was employed for an efficient wavefunction optimization. In oxygen the outer 6 electrons ($2s^2\ 2p^4$) were treated as the valence shell while for zirconium the outer 12 electrons ($4s^2\ 4p^6\ 4d^2\ 5s^2$) and for yttrium the outer 11 electrons ($4s^2\ 4p^6\ 4d^1\ 5s^2$) were treated as valence electrons. Contracted Gaussian basis sets of DZVP quality were used with a grid cutoff of 300 hartrees [19]. Although the basis sets had been optimised to reduce the basis set superposition contributions (BSSE) to the system energy, these have been taken into account when comparing energies. The counterpoise correction method of Boys and Bernardi [20] was used in which the energies are adjusted to take into account the lowering of the energy caused by the overlap of basis functions between neighbouring atoms. This correction is applied by correcting for the difference in energy between isolated atoms and the energy of these atoms when the basis sets of all the other atoms in a particular structure are included without the atoms themselves (referred to as "ghost" atoms). This gives a good approximation of the energy lowering that results solely from the overlap of basis sets between nearby atoms. The corrections were calculated for each non-equivalent atom in each of the different atomic environments, since the BSSE can depend strongly on the disposition of the surrounding atoms.

For the comparative calculations using the plane waves code VASP [21–25] full structure optimisations were carried out (using the flag ISIF = 3 for bulk phases, which relaxes the cell shape and volume in addition to the atom positions, or ISIF = 2 for molecules, which relaxes the atom positions without altering the cell shape) with no symmetry constraints (with the flag ISYM = 0 which suppresses the symmetrisation of charge densities and forces). A plane wave cut off of 600 eV was used with suitably dense Monkhost–Pack *k*-point sampling meshes for the bulk materials while atom calculations were carried out at the gamma-point in a 20 Å cubic box. Gaussian smearing of the electron occupations was applied (selected using the flag ISMEAR = 0) with a broadening of 0.05 eV (the flag SIGMA = 0.05 was used to set the width of the smearing).

The molecular dynamics simulations were carried out in the Born–Oppenheimer approximation using a time step of 0.5 fs with the Always Stable Predictor–Corrector (ASPC) method [26] in a constant pressure and temperature ensemble, thus allowing full flexibility of the simulation cells. The Canonical Sampling through Velocity Rescaling (CSVR) thermostat–barostat [27] was used with time constant of 10 fs for equilibration and accelerated dynamics and 1000 fs for molecular dynamics simulations. The barostat allows the simulation cells to change volume and shape during the simulations, thus avoiding exaggerated stresses as the hydrogen atom diffuses. The temperature was set at 1500 K for the dynamic simulations, corresponding to the extremes of temperature that could be encountered under coolant loss, while zircaloy cladding surfaces in contact with coolant are normally at about 600 K.

The surface oxide layer in Zr cladding tends to incorporate the tetragonal [28,29] form of $ZrO_2$, even below the transition temperature between the monoclinic and tetragonal forms (at 1 bar the monoclinic-tetragonal transition occurs at 1173 °C while the tetragonal-cubic transition occurs at 2270 °C) at reactor operation or even coolant loss accident conditions. The starting structure used for the dynamic simulations was based on a $3 \times 3 \times 3$ supercell of a near cubic cell of tetragonal $ZrO_2$ ($a = b = 5.153$ $c = 5.303$ $\alpha = \beta = \gamma = 90.0°$ i.e. it comprises two tetragonal unit cells) with a H atom placed at the centre of a void surrounded by the same distorted cubic arrangement of oxygen atoms as the Zr atoms ($r_{O-H,1} = 2.06$ Å and $r_{O-H,2} = 2.46$ Å). To remove an electron while maintaining charge neutrality, one of the 36 Zr atoms (the one furthest from the H substitution) was substituted with a Y atom. This allows the dynamics of the proton to be investigated with a neutral simulation cell, so avoiding the volume-dependent energy offset that arises from the Ewald treatment of the charge distribution.

An initial guess for the charge density was constructed assuming formal ionic charges, i.e. $Zr^{4+}$, $Y^{3+}$, $H^+$ and $O^{2-}$ ions. On static structure optimisation the hydrogen combined with one of the closer oxygen ions to form a hydroxide ion ($r_{O-H} = 0.99$ Å), with both the oxygen and hydrogen atoms moving together about 0.5 Å from their starting coordinates. As a result, the O atom of the hydroxide formed an almost planar arrangement with the three nearest Zr ions inducing minor distortions further away. The substitution of the Y for a Zr ion introduced slight distortions in that the four oxygen ions closest to the Y were pushed to distances of 2.25 Å compared to the 2.06 Å of the closest Zr–O coordinations. The second closest Y–O coordinations were the same distance as for that Zr–O. The concentration of Y substitution is expected to have no extensive effect on the $ZrO_2$ structure as it is equivalent to 1.4 mol% $Y_2O_3$ while 4–8 mol% is required to partially or fully stabilize the cubic structure, in addition to there being no oxygen vacancies formed since the charge balance comes from the $H^+$. The energies associated with hydrogen addition and exchange of Y for Zr atoms in the 108 atom supercell are summarised in Fig. 1. The exchange of one Y atom for a Zr atom and the addition of a hydrogen atom to $Zr_{36}O_{72}$ to form the isoelectronic $Zr_{35}YO_{72}H$ is associated with a small increase in energy (+0.13 eV).

As diffusion is a relatively slow process at the timescales accessible using atomistic modelling, which is especially true of DFT based methods, it is necessary to accelerate the simulated dynamics. In this investigation we have used the Metadynamics methods [30,31] available in CP2K to force the hydrogen atom to diffuse more quickly than it would otherwise. The collective variables used for the Metadynamics were the distances along the Cartesian *x*, *y* and *z* directions between the hydrogen atoms and the centre of the $ZrO_2$ structure defined as the average of all the zirconium and oxygen centres. During the Metadynamics simulations Gaussian potentials were placed every ten steps (5 fs) of the simulation such that the hydrogen atom was stimulated to move by the potential:

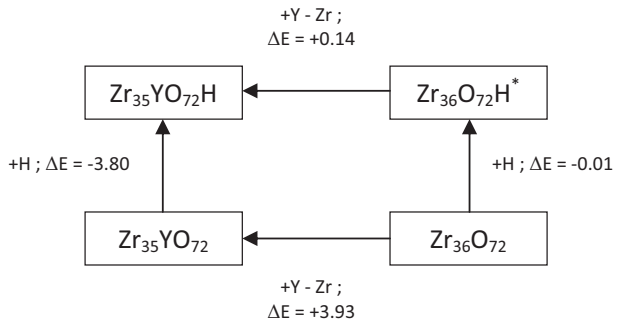


**Fig. 1.** Calculated energies for hydrogen addition and Y for Zr substitution in the tetragonal zirconia 108 atom supercell (all structures were fully optimised, spin polarised calculations were used in the two structures with an unpaired electron). *NB the structure in which a hydrogen atom is placed at an interstitial site in $ZrO_2$ is a local minimum, the structure in which an hydroxide ion is formed and the unpaired electron is accommodated in one of the other bands is 0.38 eV lower in energy.

$$V(t) = 0.01 \times \sum_{i=1}^{N(t)} \left( e^{-\frac{1}{2}\left(\frac{x(i)-x(0)}{0.01}\right)^2} \times e^{-\frac{1}{2}\left(\frac{y(i)-y(0)}{0.01}\right)^2} \times e^{-\frac{1}{2}\left(\frac{z(i)-z(0)}{0.01}\right)^2} \right)$$

where $V(t)$ is the history dependent potential, in hartrees, at timestep $t$ and $N(t)$ is the number of accumulated distance variables, $x$, $y$, and $z$, in Ångstrom. During the Metadynamics simulation this potential gradually builds up until it is sufficient to force the hydrogen atoms over any energy barriers that prevent motion. Unlike in nudged elastic band calculations, in which the start and end points of the trajectory are predetermined, the atoms in a Metadynamics simulation are free to explore the available energy landscape of the system as it undergoes both the thermal vibrations and mutual interaction with the diffusing atoms. Providing the Gaussian potentials are not so strong or placed so often that they force the whole system into an unlikely high-energy configuration, this allows energy barriers to be sampled in an unbiased manner while incorporating the thermal motions of the atoms which may open or close lower-energy diffusion pathways over time. The system trajectories and energy profiles become more complicated to interpret, however, since the thermal motion causes significant perturbations of both energy and atomic positions. By careful averaging of the system energy and identification of the points at which events start and end, it is still possible to recover reasonable estimates of the energy barrier heights along with uncertainties resulting from the thermal motion. The energies of the sampled barriers can then be used to calculate diffusion coefficients by treating the diffusion as an activated random walk.

### 1.2. Validation of simulation parameters

To assess the performance of the zirconium and yttrium pseudopotentials and DZVP basis sets employed in the CP2K calculations, the results obtained for some convenient oxide reference structures are compared with experiment and equivalent calculations using VASP in Table 1. The cohesion energies calculated with CP2K are consistently lower than those calculated with VASP because the DZVP basis sets used in CP2K, while optimised for molecules and solids, give proportionately lower atomic energies and consequently increase the apparent cohesion energies. Better agreement between the two codes is therefore obtained by comparing sublimation energies:

$ZrO_{2(cr)} \rightarrow ZrO_{2(g)} \quad \Delta E_{CP2K} = 6.91\ eV; \quad \Delta E_{VASP} = 7.03\ eV$

$Y_2O_{3(cr)} \rightarrow Y_2O_{3(g)} \quad \Delta E_{CP2K} = 8.61\ eV; \quad \Delta E_{VASP} = 8.50\ eV,$

and solid phase reactions :

$ZrO_{2(cr)} + SiO_{2(cr)} \rightarrow ZrSiO_{4(cr)} \quad \Delta E_{CP2K} = -0.12\ eV;$
$\Delta E_{VASP} = -0.18\ eV; \quad \Delta E_{exp} = -0.16\ eV$

$Y_2O_{3(cr)} + SiO_{2(cr)} \rightarrow Y_2SiO_{5(cr)} \quad \Delta E_{CP2K} = -0.83\ eV;$
$\Delta E_{VASP} = -0.72\ eV; \quad \Delta E_{exp} = -0.52\ eV$

$ZrO_{2(cr)} + 2H_2O_{(g)} \rightarrow Zr(OH)_{4(cr)} \quad \Delta E_{CP2K} = 0.09\ eV;$
$\Delta E_{VASP} = 0.10\ eV; \quad \Delta E_{exp} = 0.39\ eV$

$\frac{1}{2}Y_2O_{3(cr)} + 1\frac{1}{2}H_2O_{(g)} \rightarrow Y(OH)_{3(cr)} \quad \Delta E_{CP2K} = -0.97\ eV;$
$\Delta E_{VASP} = -0.90\ eV; \quad \Delta E_{exp} = -0.65\ eV.$

where the experimental hydration energies exclude the zero point and thermal energies of the water vapour, a combined energy of 0.65 eV per water molecule.

**Table 1**
Cohesion energies calculated using CP2 K (corrected for BSSE) and VASP compared with experiment.

| | Cohesion energy (eV) | | |
|---|---|---|---|
| | CP2K | VASP | Expt. |
| $ZrO_{2(cr)}$ monoclinic | −22.08 | −23.59 | −22.77 [32] |
| $ZrO_{2(cr)}$ tetragonal | −21.97 | −23.48 | ∼−22.71 [32] |
| $ZrO_{2(cr)}$ cubic | −21.85 | −23.38 | – |
| $ZrO_{2(g)}$ [b] | −15.17 | −16.55 | – |
| $Zr(OH)_{4(cr)}$ [a] | −41.67 | −44.41 | −42.91 [33] |
| $ZrSiO_{4(cr)}$ | −40.53 | −43.62 | −42.26 [32] |
| $Y_2O_{3(cr)}$ | −34.67 | −36.93 | −36.28 [32] |
| $Y_2O_{3(g)}$ [b] | −26.06 | −28.43 | – |
| $Y(OH)_{3(cr)}$ | −66.13 | −70.13 | −68.37 [34] |
| $Y_2SiO_{5(cr)}$ | −53.82 | −57.50 | −56.13 [35] |
| $H_2O_{(g)}$ | −9.84 | −10.46 | −9.61 [32] |
| $SiO_{2(cr)}$ | −54.97 | −19.85 | −19.33 [32] |

[a] As generally prepared, $Zr(OH)_4$ is amorphous and hydrated [36] so for the calculations a crystalline structure based on monoclinic $ZrF_4$ was used. On optimisation a low symmetry structure ($P\bar{1}$) was adopted in which some hydroxide ions had rearranged to oxide ions and water leaving two thirds of the Zr ions in sevenfold coordinations. The experimental cohesion energy is derived from the Gibbs energy given in the cited reference using a simple estimate for the entropy of formation.

[b] For the $ZrO_2$ molecule the bent configuration was used (relaxed structure $r_{Zr-O}$ = 1.802 Å; $\theta_{O-Zr-O}$ = 105.95°) while for the $Y_2O_3$ molecule the Y atoms capped an equilateral triangle of O atoms (relaxed structure $r_{Y-O}$ = 2.077 Å; $r_{O-O}$ = 2.700 Å; $\theta_{Y-O-Y}$ = 82.76°).

## 2. Results

Fig. 2 shows a plot of the potential energy and Fig. 3 shows projections of the hydrogen atom trajectory during the 0.5 ps molecular dynamics simulation. Even without the accelerated dynamics, the hydrogen moved from the initially bound oxide ion to an adjacent oxide ion.

Figs. 4 and 5 show the equivalent plots for the 3 picoseconds of accelerated dynamics, wherein four more diffusion events were sampled.

From the trajectories it is observed that the diffusion of the hydrogen atom is mediated by the close approach of pairs of O atoms. At each moment that the hydrogen atom moved from one oxygen atom to another a bridging O–H–O unit was formed with $r_{OH}$ = 1.26 ± 0.07 Å, and the oxygen atoms approached to within 2.52 Å compared to the average O–O separation from the simulations of 2.75 Å (for comparison the amplitude of the H oscillations was about 0.17 Å). The approach of oxygen atoms to within this range accounts for 6% of the first peak in the averaged O–O radial distribution function. If it is assumed that the O–H bond is randomly orientated independent of the local oxygen atoms then the likelihood of two oxygen atoms approaching within this range

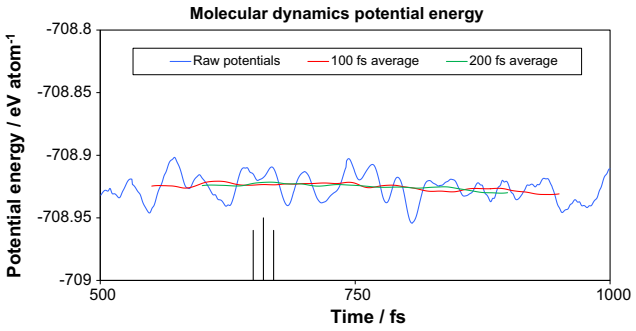


**Fig. 2.** Potential energy of the system (blue line) and rolling averages over 100 femtoseconds (red line) and 200 femtoseconds (green line) during molecular dynamics. The black lines show where the hydrogen atom moves from one oxygen atom to another. (For interpretation of the references to colour in this figure legend, the reader is referred to the web version of this article.)

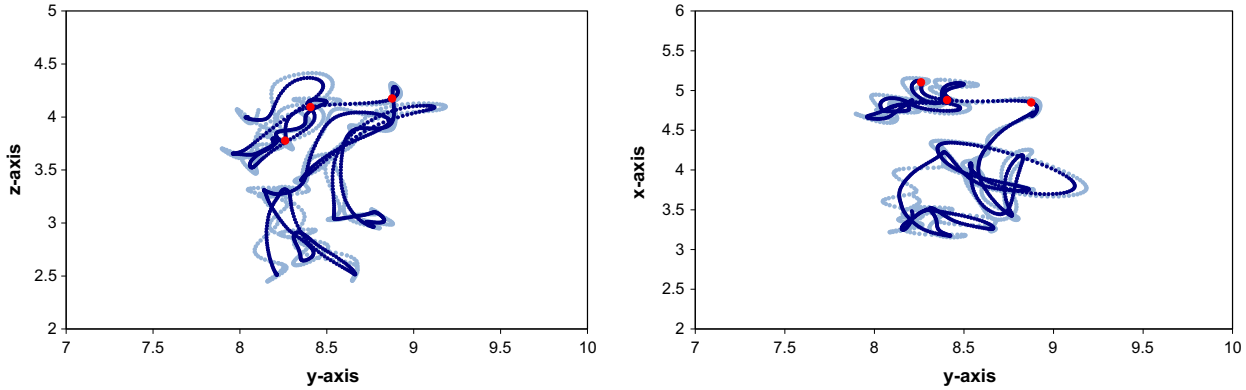


**Fig. 3.** Coordinates of the hydrogen atom during molecular dynamics projected on the Cartesian *yz* (left) and *yx* (right) planes. The red circles mark the start, middle and end hydrogen diffusion event. The pale blue points show the raw coordinates while the darker blue points are 10 fs rolling averages to mask the high-frequency H–O vibrations. (For interpretation of the references to colour in this figure legend, the reader is referred to the web version of this article.)

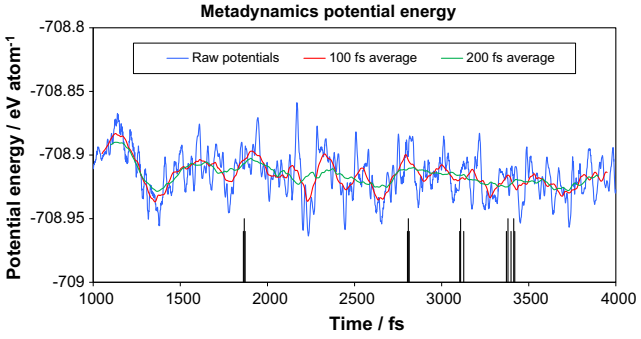


**Fig. 4.** Potential energy of the system (blue line) and rolling averages over 100 femtoseconds (red line) and 200 femtoseconds (green line) during accelerated dynamics. The black lines show where the hydrogen atom moves from one oxygen atom to another. (For interpretation of the references to colour in this figure legend, the reader is referred to the web version of this article.)

with the H between them (i.e. O–H–O < 15°) is reduced to about 0.1%. Fig. 6 plots the distances of the two oxygen atoms closest to the hydrogen atom during the accelerated dynamics. Although there were several points where the hydrogen oxygen distances were close enough to allow the hydrogen atom to move from one oxygen to another (O–H < 1.33 Å), this did not always occur. There are also several instances where the hydrogen does move from one oxygen atom to another but then moves back to the initial oxygen atom within a few femtoseconds.

Fig. 7 shows a plot of the electron density difference between the system at the midpoint of the first diffusion event of the accelerated dynamics (1867 fs) and the same system with the hydrogen removed (as a proton). At this instant the buildup of charge around the hydrogen gives it a Bader charge of 0.5 electrons (i.e. an atomic charge of +0.5), the charge of the two adjacent oxygen atoms is the same as those of the rest of the lattice. In the statically optimised structure, the Bader method does not associate any charge with the hydrogen atom (i.e. it has a charge of +1) while the bonded oxygen has 0.4 electrons more that the other oxygen atoms. Charges from the Mulliken population analysis throughout the simulations associate about 0.2 electrons of charge with the hydrogen, and on the bonded oxygen about 0.2 electrons less the other oxygen atoms. At the middle of the diffusion event there is no significant change in the Mulliken charge of the hydrogen, while the charges on the two oxygen atoms are equal. The molecular orbitals from the calculation confirm the presence of a three-centre-two-electron bond at the midpoint of the diffusion step.

Table 2 gives the energy barriers and calculated diffusion coefficients for the diffusion events sampled during the molecular dynamics and accelerated dynamics. Two sets of values are given using averaging periods for the potential energy of 100 fs and 200 fs respectively.

It is difficult to disentangle the trends in potential energy caused by the global system dynamics from the interactions local to the hydrogen atom owing to the short timespan of the diffusion events. One can also note that some variation in the energy barriers is to be expected in any case since the environments local to the hydrogen atom are permanently changing. It is clear that the H diffusion has a low energy barrier of the order 100 meV and a diffusion coefficient of around $4 \times 10^{-9}/m^2\,s^{-1}$ at 1500 K.

Experimental studies of hydrogen diffusion in $ZrO_2$ oxides give a wide range of activation energies, 0.17–1.6 eV [37–40], while recent static DFT calculations [9] place the barrier even higher at 2.1 eV. An investigation of water uptake in yttrium stabilized zirconia [8] indicated hydrogen diffusivities of $8 \times 10^{-11}/m^2\,s^{-1}$ at 890 °C and $1.3 \times 10^{-10}/m^2\,s^{-1}$ at 990 °C. The value of the calculated diffusion coefficient carries relatively large uncertainty (±80%) owing to the relatively large uncertainties in the low energy barriers caused by the overall oscillations in the system potential energy and the small number of diffusion events that were sampled. The prefactors used to calculate the diffusion coefficient are also a source of uncertainty because of the difficulty in differentiating between motion associated with the diffusion of hydrogen, i.e. moving between oxygen atoms, motion where the hydrogen remains bonded to the same oxygen but swivels around it, and the high-frequency oscillations of the O–H bond. In the calculated coefficients the sampled energy barriers are combined with the distance travelled at the same time, i.e. the jump between oxygen atoms. Using 10 fs averages of the H atom coordinates rather than the raw coordinates (Figs. 3 and 5), which is sufficient to remove most of the high-frequency vibrations, alters the diffusion coefficient values by about 10%. The displacement associated with H–O swivelling was up to twice the H–O bond distance (about 2 Å) and often occurred after the H moved between oxygen atoms, the momentum of the diffusing H atom contributing to the swivelling motion. Between the diffusion events there was sufficient time for complete re-orientation of the H–O bond to occur.

The formation of a three-centre-two-electron bond in the O–H–O transition states is partly responsible for the low energy barrier for the H diffusion and is why the hydrogen atom only

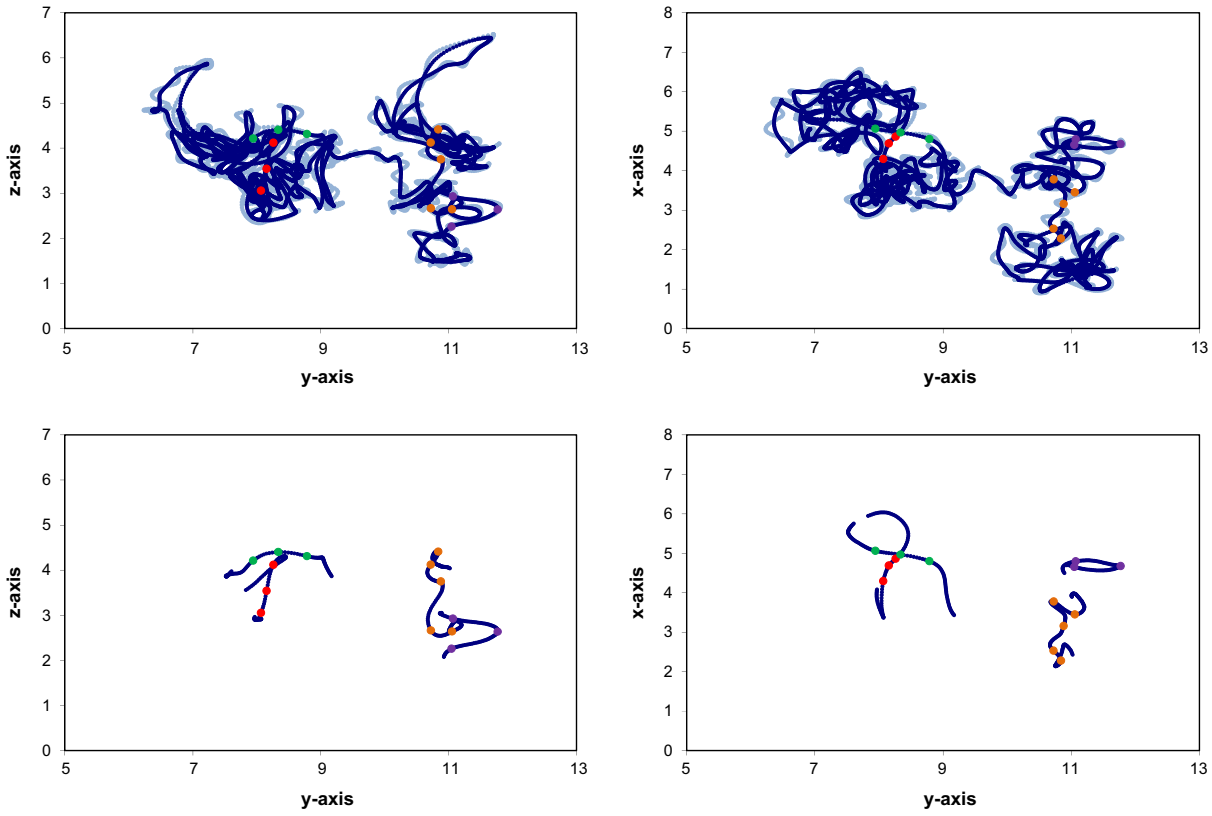


**Fig. 5.** Coordinates of the hydrogen atom during accelerated dynamics projected on the Cartesian *yz* (left) and *yx* (right) planes. The coloured circles mark the four hydrogen diffusion events in the order red, green, purple, orange. The top row shows the raw coordinates in pale blue and the 10 fs rolling averages to mask the high-frequency H–O vibrations in dark blue. The bottom row shows the four 50 fs segments of the trajectory around the diffusion events for clarity. (For interpretation of the references to colour in this figure legend, the reader is referred to the web version of this article.)

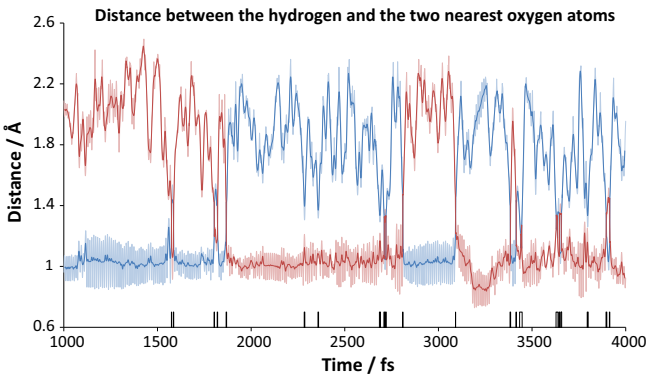


**Fig. 6.** Distance between the hydrogen and the two nearest oxygen atoms during accelerated dynamics. The pale lines show the actual distances while a darer shade shows a 10 fs rolling average that hides the higher-frequency H–O vibrations. Where the identities of the nearest oxygen atom changes, the red and blue colours are swapped. The black lines indicate where the two H–O distances are simultaneously less than 1.33 Å. (For interpretation of the references to colour in this figure legend, the reader is referred to the web version of this article.)

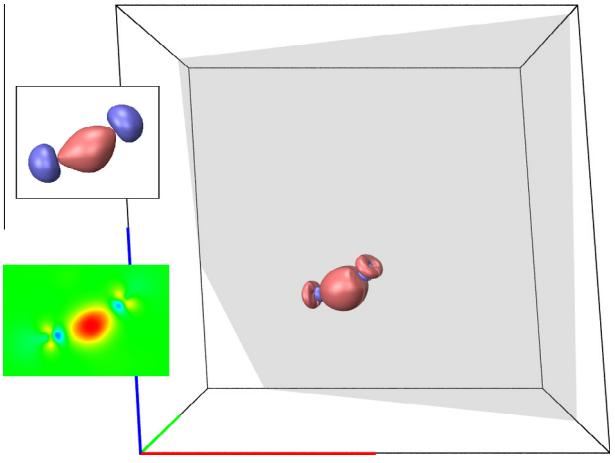

**Fig. 7.** Isosurface plot of the electron density difference between the protonated and deprotonated system (both systems have the same number of electrons i.e. the deprotonated system carries charge of −1 per supercell) at the moment the hydrogen moves from one oxygen to another (1867 fs). The pink parts of the isosurface are where the electron density difference is positive and blue where it is negative. The upper inset shows a plot of the main Kohn–Sham orbital of the O–H–O bond and the lower inset shows a close-up of the density difference in the slice shown in grey. (For interpretation of the references to colour in this figure legend, the reader is referred to the web version of this article.)

jumps between pairs of oxygen atoms when they approach one another. Calculations of an isolated $OH^-$ ion show that the separation of a hydroxide ion into an oxide ion and a proton requires a very high energy, about 29.3 eV. The energies involved when a hydrogen atom moves between two oxygen atoms in the isolated $OHO^{3-}$ ion are very much lower. When the oxygen atoms are fixed at 2.75, 2.64 and 2.50 Å apart then the energy barriers for hydrogen moving between the oxygen atoms are 140, 50 and 0 meV respectively. Note that although there is no energy barrier once the oxygen atoms approach to 2.5 Å, there is a significant energy increase associated with bringing the oxygen atoms together (the equilibrium separation of the oxygen atoms in the free ion $OHO^{3-}$ is 3 Å).

**Table 2**
Barrier heights and calculated diffusion coefficients for the events occurring during the molecular dynamics and Metadynamics simulations.

| Barrier midpoint (fs) | Energy barrier (meV) | | Diffusion coefficient $\times 10^9$ ($m^2\ s^{-1}$) | |
|---|---|---|---|---|
| | 100 fs mean ± 128 | 200 fs mean ± 112 | 100 fs mean | 200 fs mean |
| 660 | 49 | 86 | $2.15^{+0.99}_{-1.35}$ | $1.55^{+0.90}_{-1.46}$ |
| 1867 | 55 | 24 | $5.75^{+3.03}_{-3.62}$ | $6.20^{+1.26}_{-3.59}$ |
| 2809 | 0 | 60 | $5.21^{+0.00}_{-3.28}$ | $2.49^{+1.47}_{-1.44}$ |
| 3109 | 167 | 7 | $0.64^{+1.09}_{-0.40}$ | $2.24^{+1.20}_{-1.30}$ |
| 3381 | 132 | 261 | $8.05^{+13.7}_{-5.07}$ | $3.02^{+4.16}_{-1.75}$ |

## 3. Conclusion

Metadynamics simulations using DFT calculate an energy barrier of about 125 meV for the diffusion of protons through the tetragonal zirconia structure at 1500 K. The corresponding value for the diffusion coefficient of $4 \times 10^{-9}/m^2\ s^{-1}$ is somewhat higher than expected from an Arrhenius fit of the measured diffusion rates [41], which gives a value of $3.2 \times 10^{-10}/m^2\ s^{-1}$. However, this simulation is not by itself sufficient to obtain a definitive diffusion rate that is directly comparable with the experimentally measured values. Since the diffusion of protons constitutes an electric current, for continuous diffusion to occur there would have to be a counter current that prevents a build-up of charge. Hence, the slower measured diffusion rates could be attributed to trapping of hydrogen in defect sites or to a concurrent diffusion of oxygen ions to balance the charge current associated with proton diffusion. The measured diffusion coefficient of oxygen in tetragonal zirconia [42] is about $10^{-12}/m^2\ s^{-1}$ around 1200 °C (i.e. 1473 K).

The proton diffusion is apparently limited by the lattice vibrations insofar as hydrogen diffusion only occurs in the simulations when the oxygen atoms are about 2.5 Å apart. The presence of a three-centre bond at the moment that hydrogen atoms transition between pairs of oxygen atoms in DFT calculations, combined with the very high energy associated with separating a proton from an isolated hydroxide ion, point to this interaction being a significant factor for the much faster diffusion rates in tetragonal zirconia of protons compared to neutral hydrogen atoms.

The mechanisms for the reaction of water with zirconia published in the literature [e.g. Veshchunov] have referred to protons adsorbed on or absorbed in the oxide phase. In light of the results from these DFT calculations we can be more specific and refer to these species as hydroxide ions. One could go further and note that the surfaces of zirconia before steam ingress are likely to contain free metal coordinations which can bond to water which can then react with nearby oxide ions to form hydroxide ions on the surface. Diffusion of the hydrogen from the surface hydroxide ions into the bulk would then be able to occur rapidly, albeit restrained by the rate at which the balancing charge in the form of oxide ions diffuse. This also explains the relative unimportance of the reduction of hydrogen at the oxide surface [1] and the observed rates of hydrogen transport through the oxide to the zirconium alloy [41,43].

The interaction of zirconium based cladding materials with steam under accident conditions is a complicated process involving several material phases [43,44]. The morphology of the surface oxide layer is also a consideration for studies of hydrogen uptake [45]. The difficulty of isolating the parameters of any one process in the presence of numerous influences is assisted by atomistic modelling. While experimental measurements are influenced by material defects, such as cracks and crystal boundaries, and in the case of proton diffusion in zirconia by the presence of a charge balancing current, atomistic simulations can be contrived to circumvent such effects. When comparing results between simulation and experiment in such cases it is essential to bear in mind the influence that the circumvented effects could have. The solubility of protons in zirconia is also an important factor in the transport of hydrogen through the oxide layers of zircaloys since the proton flux is a function of both diffusion rate and concentration. A study of proton solubility using atomistic methods is complicated by the necessity to maintain charge balance or suffer large, fictitious contributions to the system energy. The method employed in this work, namely replacing Zr atoms with Y atoms to balance charges, would be of little use for an investigation of solubility. In fact, realistic solutions would require large simulation cells such as where the dissociation of water molecules to give protons and hydroxide/oxide at the zirconia surfaces could be investigated adequately.

## References


[1] M.S. Veshchunov, A.V. Berdyshev, J. Nucl. Mater. 255 (1998) 250–262.
[2] J. Böhmert, M. Dietrich, J. Linek, Zentralinstitut für Kernforschung, Rossendorf dei Dresden, 1991.
[3] J. Böhmert, M. Dietrich, J. Linek, Nucl. Eng. Design 147 (1993) 53–62.
[4] V.I. D'yachkov, Zh. Prikladnoi Khimii 64 (1991) 2029–2036.
[5] J. Frecska, G. Konczos, L. Maróti, L. Matus, KFKI Atomic Energy Research Institute, 1995.
[6] V. Vrtilkova, L. Molin, K. Kloc, V. Hamouz, Voprosy Atomnoj Nauki I Tehniki 27 (1988) 84–89.
[7] K. Park, D.R. Olander, J. Am. Ceram. Soc. 74 (1991) 72–77.
[8] C. Wagner, Ber. Bunsenges. Phys. Chem. 72 (1968) 778–781.
[9] H. Muta, Y. Etoh, Y. Ohishi, K. Kurosaki, S. Yamanaka, J. Nucl. Sci. Technol. 49 (2012) 544–550.
[10] M. Krack, M. Parrinello, Quickstep: make the atoms dance, in: J. Grotendorst (Ed.), High Performance Computing in Chemistry, NIC-Directors, 2004.
[11] J. VandeVondele, M. Krack, F. Mohamed, M. Parrinello, T. Chassaing, J. Hutter, Comput. Phys. Commun. 167 (2005) 103–128.
[12] http://www.cp2k.org2000-2012.
[13] G. Lippert, J. Hutter, M. Parrinello, Mol. Phys. 92 (1997) 477–487.
[14] J.P. Perdew, K. Burke, M. Ernzerhof, Phys. Rev. Lett. 77 (1996) 3865–3868.
[15] S. Goedecker, M. Teter, J. Hutter, Phys. Rev. B 54 (1996) 1703–1710.
[16] C. Hartwigsen, S. Goedecker, J. Hutter, Phys. Rev. B 58 (1998) 3641–3662.
[17] M. Krack, Theor. Chem. Acc. 114 (2005) 145–152.
[18] J. VandeVondele, J. Hutter, J. Chem. Phys. 118 (2003) 4365–4369.
[19] J. VandeVondele, J. Hutter, J. Chem. Phys. 127 (2007) 114105.
[20] S.F. Boys, F. Bernardi, Mol. Phys. 19 (1970) 553–566.
[21] G. Kresse, J. Furthmüller, Phys. Rev. B 54 (1996) 11169–11186.
[22] G. Kresse, J. Furthmüller, Comput. Mater. Sci. 6 (1996) 15–50.
[23] G. Kresse, J. Hafner, Phys. Rev. B 47 (1993) 558–561.
[24] G. Kresse, J. Hafner, Phys. Rev. B 49 (1994) 14251–14269.
[25] G. Kresse, D. Joubert, Phys. Rev. B 59 (1999) 1758–1775.
[26] J. Kolafa, J. Compd. Chem. 25 (2004) 335–342.
[27] G. Bussi, D. Donadio, M. Parrinello, J. Chem. Phys. 126 (2007) 014101.
[28] H. Anada, K. Takeda, in: 11th Int. Symposium on Zirconium in the Nuclear Industry, 1996, pp. 35–54.
[29] H.G. Beie, A. Mitwalsky, F. Garzarolli, H. Ruhmann, H.J. Sell, in: 10th Int. Symposium on Zirconium in the Nuclear Industry, 1994, pp. 615–643.
[30] M. Iannuzzi, A. Laio, M. Parrinello, Phys. Rev. Lett. 90 (2003) 238302.
[31] A. Laio, M. Parrinello, Proc. Natl. Acad. Sci. USA 99 (2002) 12562–12566.
[32] D.R. Lide, H.V. Kehiaian, CRC Handbook of Thermophysical and Thermochemical Data, CRC Press, 1994.
[33] L. Qiu, D.A. Guzonas, D.G. Webb, J. Solut. Chem. 38 (2009) 857–867.
[34] I.I. Diakonov, K.V. Ragnarsdottir, B.R. Tagirov, Chem. Geol. 151 (1998) 327–347.
[35] J.-J. Liang, A. Navrotsky, T. Ludwig, H.J. Seifert, F. Aldinger, J. Mater. Res. 14 (1999) 1181–1185.
[36] C. Huang, Z. Tang, Z. Zhang, J. Am. Ceram. Soc. 84 (2001) 1637–1638.
[37] J.H. Austin, T.S. Elleman, K. Verghese, J. Nucl. Mater. 51 (1974) 312–329.
[38] D. Khatamian, J. Alloys Compd. 253–254 (1997) 471–474.
[39] D. Khatamian, F.D. Manchester, J. Nucl. Mater. 166 (1989) 300–306.
[40] W. Kunz, H. Munzel, U. Kunz, J. Nucl. Mater. 136 (1985) 6–15.

[41] M.S. Veshchunov, V.E. Shestak, Nucl. Eng. Des. 252 (2012) 96–107.
[42] K. Park, D.R. Olander, J. Electrochem. Soc. 138 (1991) 1154–1159.
[43] M. Große, M. Steinbrück, E. Lehmann, P. Vontobel, Oxid. Met. 70 (2008) 149–162.
[44] M. Große, E. Lehmann, M. Steinbrück, G. Kühne, J. Stuckert, J. Nucl. Mater. 385 (2009) 339–345.
[45] M. Große, M. Steinbrück, J. Stuckert, A. Kastner, B. Schillinger, J. Mater. Sci. 47 (2012) 6505–6512.